Advanced Composite Materials
Publication details, including instructions for authors and subscription information:
http://www.tandfonline.com/loi/tacm20

# Void formation in geometry-anisotropic woven fabrics in resin transfer molding

Ryosuke Matsuzaki[a], Daigo Seto[b], Akira Todoroki[b] & Yoshihiro Mizutani[b]

[a] Department of Mechanical Engineering, Tokyo University of Science, 2641 Yamazaki, Noda, Chiba, 278-8510, Japan.

[b] Department of Mechanical Sciences and Engineering, Tokyo Institute of Technology, 2-12-1 O-okayama, Meguro, Tokyo, 152-8552, Japan.

Published online: 25 Aug 2013.

To cite this article: Ryosuke Matsuzaki, Daigo Seto, Akira Todoroki & Yoshihiro Mizutani (2014) Void formation in geometry-anisotropic woven fabrics in resin transfer molding, Advanced Composite Materials, 23:2, 99-114, DOI: 10.1080/09243046.2013.832829

To link to this article: http://dx.doi.org/10.1080/09243046.2013.832829

*Advanced Composite Materials*, 2014
Vol. 23, No. 2, 99–114, http://dx.doi.org/10.1080/09243046.2013.832829



# Void formation in geometry–anisotropic woven fabrics in resin transfer molding

Ryosuke Matsuzaki[a]*, Daigo Seto[b], Akira Todoroki[b] and Yoshihiro Mizutani[b]

[a]*Department of Mechanical Engineering, Tokyo University of Science, 2641 Yamazaki, Noda, Chiba 278-8510, Japan;* [b]*Department of Mechanical Sciences and Engineering, Tokyo Institute of Technology, 2-12-1 O-okayama, Meguro, Tokyo 152-8552, Japan*

(*Received 13 May 2013; accepted 6 August 2013*)

When geometry–anisotropic fabrics, in which the thickness and width of fiber bundles differ in the warp direction and weft direction, respectively, are used for resin transfer molding (RTM), microscopic porous structures along a flow path may depend on the resin flow direction. This study investigated the influence of woven fabrics' geometric anisotropy on inter-bundle void formation due to air entrapment at the flow front during RTM. The void content–resin flow velocity relationship was measured in warp (narrow and thick bundle) and weft (wide and thin bundle) directional impregnation. In experiments, warp directional impregnation indicated higher critical resin flow velocity of void formation and void content under a given resin flow velocity than in weft directional impregnation. Void formation was also largely affected by capillary fingering, where warp directional impregnation indicated a higher critical flow velocity of fingering formation. This may be because the gap between the fiber bundle and the mold surface is smaller in the warp direction; thus, the capillary force is higher, and fingering is facilitated compared with weft directional impregnation. Additionally, this may lead to a higher critical velocity of void formation and higher void content at a given flow velocity in warp directional impregnation.

**Keywords:** resin transfer molding; void; impregnation; glass fiber; polyester resin; anisotropy



## 1. Introduction

Resin transfer molding (RTM) reduces manufacturing and material costs because the process does not require an expensive autoclave and prepregs.[1] However, owing to the complex porous structures of woven fabrics, configuration of the flow front tends to be complicated. This often leads to void formation.[2,3] Because the voids that remain in the structure degrade the properties of the composites,[4–6] the application of RTM is currently limited to parts that do not require high reliability. For broader RTM adoption, it is essential to understand the processes of void generation and suppression during RTM.

Voids formed during RTM are classified as macro-, meso-, and micro-voids, depending on their scale. Macro-voids, also called dry spots, are large-scale voids that are formed by incomplete resin filling, and they are cured in an unimpregnated state.[7,8]

*Corresponding author. Email: rmatsuza@rs.tus.ac.jp

In contrast, meso- and micro-voids are small bubbles that are generated due to air entrapment at the flow front because of fabrics' microscopic structure. Meso-scale voids are those that are trapped between fiber bundles, whereas micro-voids are located inside bundles.[9–12] In this study, we focus on meso-voids that remarkably increase the void content of molded parts among meso- and micro-voids.

It is well known that the void content depends on the flow front velocity or capillary number $Ca^*$,[8,13–16] and the relationship between void content and capillary number varies depending on fabric architecture.[9,16] This is because different fabric architectures (e.g. woven patterns, porous structures, or fiber volume fraction) generate different microscopic resin flow paths. However, thus far, a unified formulation for explaining the effect of fabric architecture on void generation has not been developed.

For developing a unified formulation, it is essential to know the influence of geometrical parameters of the fabric architecture on void formation. Therefore, the present study focused on geometry–anisotropic plain woven fabrics. In the case of plain-woven fabrics with isotropic permeability, the relationship between the void content and flow velocity is the same in the weft and warp directions. However, among plain-woven fabrics, there exist permeability-anisotropic fabrics even though the fabrics have isotropic mechanical properties. Because woven fabrics are generally manufactured as long, rectangular sheets, which are shipped as rolls, a difference may arise in the thickness and width of the fiber bundles in the circumferential direction (the warp direction) and the shaft direction (the weft direction) of the roll during manufacturing. When geometry–anisotropic fabrics, in which the thickness and width of the fiber bundles differ between the warp and weft directions, are used for RTM, porous structures along the flow path may change depending on the resin flow direction. This affects resin flow progress and void formation. Therefore, it is essential to consider the resin impregnation direction in addition to the flow velocity for predicting void formation.

Based on the above background, the present study focused on geometry–anisotropic fabrics and evaluated the influence of the impregnation direction on the relationship between the void content and the resin flow velocity, which are important parameters in optimizing the resin impregnation process of RTM. However, conventional void content measurements, such as cross-sectional observation, combustion methods, and buoyancy measurements use the molded parts obtained after resin curing.[9,11,12,15–17] Consequently, the measured void content includes the influence of void transportation, cure shrinkage, diffusion to resin, etc.[9,18–20] in addition to air entrapped due to the microstructure of the woven fabric focused on in this study. Therefore, an *in situ* method of measuring void content during impregnation [21] was used for appropriately evaluating the influence of void trapping. Based on the *in situ* void observation, the present study investigated the geometry–anisotropic effects of woven fabrics on the behavior of resin progress and void formation during RTM.

## 2. Geometry–anisotropic woven fabrics

Because woven fabrics are manufactured as long, rectangular sheets, a difference may arise in the geometry of fiber bundles in the warp and weft directions. Figure 1 shows examples of geometry–anisotropic plain-woven fabrics, M100K104 (Unitika Glass Fiber Co.) and YEM1801 (Solar Co.). The thickness and width of the fiber bundles differ in the warp direction and the weft direction for both fabrics. That is, narrow and thick fiber bundles are used in the warp direction, whereas wide and thin fiber bundles are used in the weft direction. Consequently, these woven fabrics have geometric

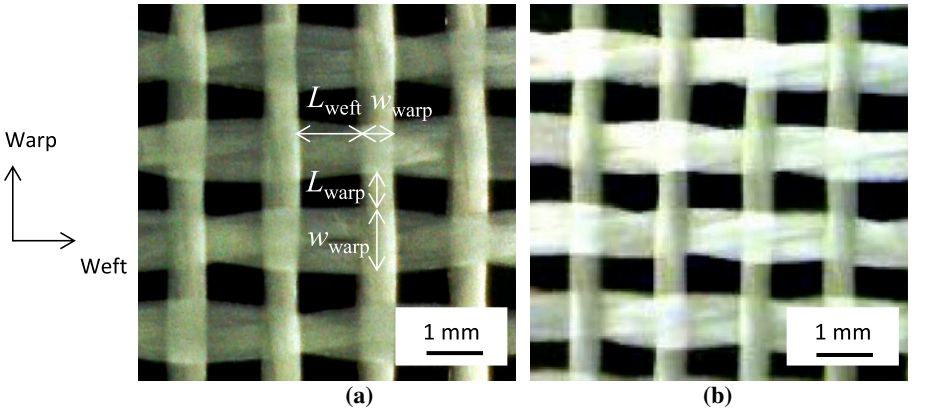


Figure 1. Geometry–anisotropic plain woven fabric. (a) M100K104 and (b) YEM1801 composed of various configurations of bundles in warp and weft directions.

anisotropy. Table 1 shows the material properties of geometry–anisotropic woven fabrics of YEM1801 and M100K104. The porosity inside a single fiber bundle was determined by analyzing the cross-sectional image of the fiber bundle using image analysis software (NI Vision Assistant 8.5, National Instruments).

Note that for both the woven fabrics, the number of fiber bundles per unit length (namely, center-to-center distance of fiber bundles), filament number contained in a single fiber bundle, and cross-sectional area ($\pi$ $w$ $h$/4) of the bundle are identical in the warp and weft directions. However, the width:height ratio, i.e. the aspect ratio ($h$/$w$), of the fiber bundles differs. Therefore, because the porous structures in the bundle are the same in the warp and the weft, the capillary pressure in the fiber bundle is the same in the warp and weft directions. In addition, there is almost no difference in the mechanical properties such as tensile strength and stiffness in the warp and weft directions. However, because of geometric anisotropy due to the difference in the thicknesses of the weft and warp fiber bundles, the configuration of the gaps in the woven network

Table 1. Material properties of geometry–anisotropic fabrics.

| | Value (coefficient of variation) | |
|---|---|---|
| Variable | M100K104 | YEM1801 |
| Thickness of fiber mat $H$ [m] | [a]$1.4 \times 10^{-4}$ | [a]$1.7 \times 10^{-4}$ |
| Superficial porosity of fiber mat $\Phi$ | 0.18 | 0.24 |
| Number of fiber bundles [/25 mm] | [a]19 | [a]19 |
| Distance between bundles in warp direction $L_{warp}$ [m] | $4.1 \times 10^{-4}$ | $5.1 \times 10^{-4}$ |
| Distance between bundles in weft direction $L_{weft}$ [m] | $7.1 \times 10^{-4}$ | $7.2 \times 10^{-4}$ |
| Height of fiber bundle in warp direction $h_{warp}$ [m] | $8.4 \times 10^{-5}$ (10%) | $9.8 \times 10^{-5}$ (10%) |
| Height of fiber bundle in weft direction $h_{weft}$ [m] | $5.6 \times 10^{-5}$ (7%) | $7.2 \times 10^{-5}$ (6%) |
| Width of fiber bundle in warp direction $w_{warp}$ [m] | $5.9 \times 10^{-4}$ (5%) | $5.8 \times 10^{-4}$ (7%) |
| Width of fiber bundle in weft direction $w_{weft}$ [m] | $8.9 \times 10^{-4}$ (13%) | $7.9 \times 10^{-4}$ (9%) |
| Number of fibers inside bundles $n$ | [a]400 | 400 |
| Porosity inside bundles $\phi$ | 0.37 (5%) | 0.34 (8%) |
| Fiber radius $r$ [μm] | 4.2 (7%) | 4.8 (4%) |

[a]Indicates the data provided by manufacturer.

varies depending on the direction of the resin impregnation. Thus, the behaviors of resin impregnation and void formation differ in the warp and weft directions.

## 3. Relationship between resin flow velocity and void content

### 3.1. Experimental

The effect of anisotropic geometry of woven fabrics on the relationship between void content and flow velocity was experimentally investigated in the case of warp and weft directional impregnation of one-dimensional RTM. The void content was measured *in situ* to evaluate the void content that was simply due to air-trapping caused by the microstructure of the woven fabrics in their respective locations, thus disregarding the effects of void transportation, migration, and diffusion.

Figure 2 shows the experimental apparatus used for visualization of the flow front and voids during the one-dimensional flow experiments. A single layer of plain-woven

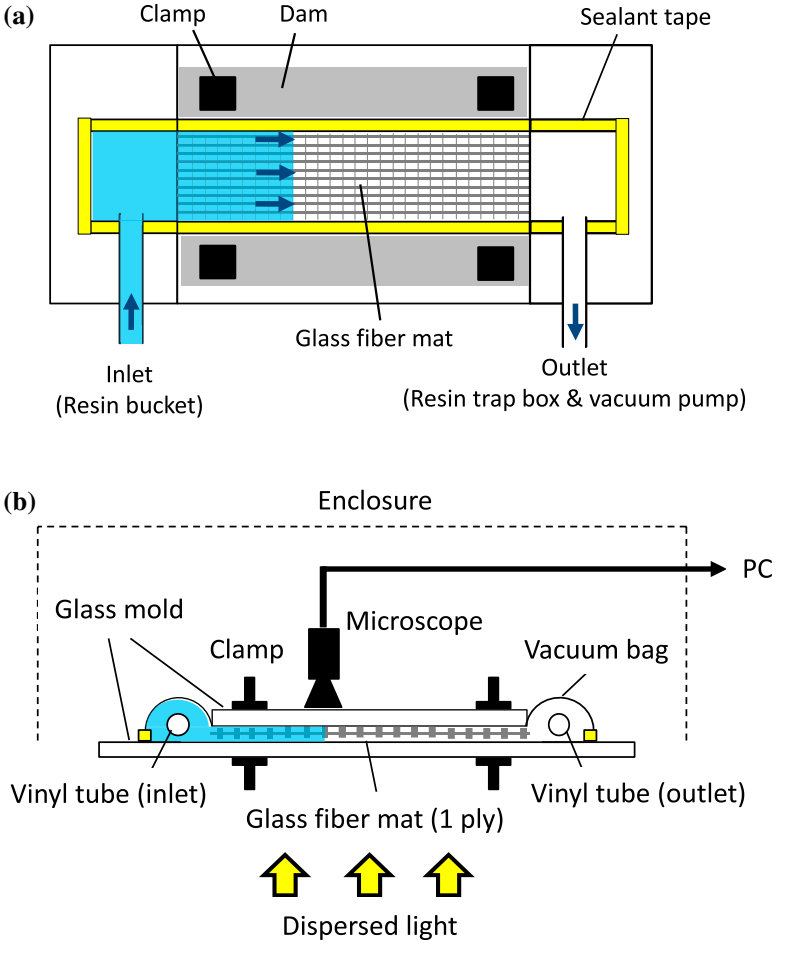


Figure 2. Experimental setup for process visualization during one-dimensional resin flow RTM. (a) Upper view. (b) Side view.

glass cloth (M100K104 or YEM1801) was used as the woven fabric, which had dimensions of $200 \times 50$ mm. The fabric was then sandwiched between two colorless transparent glass plate molds. Both longitudinal sides of the glass fabrics were sealed with sealant tape and then fixed between the glass plate molds by using clamps through insertion of glass composite dams. A curing agent (Epoch PN) was added at 1 PHR (per hundred resin) to the unsaturated polyester resin (Sundhoma PC184-C, DH Material Inc.). The resin was impregnated using negative pressure by vacuum pump. The resin flow direction and the injection pressure in the experiments are shown in Table 2. A single experiment was conducted for each condition. However, for verification purposes, we also tested other conditions not listed in Table 2, such as YEM1801/Weft/30 kPa, and the obtained results were found to be similar to those for the conditions listed in Table 2 and in terms of the relationship between the resin flow velocity and the void fraction. Therefore, in the study, we selected those conditions from among all tested conditions that were within the same flow velocity range. Note that the injection pressure indicates the differential pressure from the atmospheric pressure. The negative pressure of the vacuum pump was kept constant from the beginning of resin injection until the completion of resin curing. In the present study, we established the experimental setup by using one-layer fabric, a stiff glass mold, and a lower fiber volume fraction than that in actual production to facilitate observation of the void formation (i.e. to enlarge the void volume) caused by the architecture of the woven fabric. Moreover, a low injection pressure was used because it gives a low pressure gradient without having to use large specimens.

A digital microscope (M3, Scholar) was installed on the upper surface of the mold, and a photograph of the impregnation behavior at the flow front was taken at distances of $x = 25$, 50, 75, 100, 125, 150, and 175 mm from the resin inlet. The images obtained by the microscope at the point of air-trapping were processed and analyzed with image analysis software (Vision Assistant 8.5, National Instruments). A representative image of the visualized void is shown in Figure 3. Because the fiber bundles seemed to disappear owing to their impregnation with resin, both the flow front and the voids were clearly observed, and the void content could be easily calculated via image analysis. The measurement area was set as a $5 \times 15$ mm rectangular area at each measurement location, where the longitudinal direction of the rectangular area was consistent with the direction perpendicular to resin flow. This is because in a one-dimensional flow, conditions such as flow velocity and pressure are constant along a direction perpendicular to the resin flow. The area ratio of the void content at each location was then calculated. It is assumed that the voids had a columnar shape because the fabric used in

Table 2. Experimental conditions of flow directions and injection pressure.

| Woven fabric | Flow direction | Injection pressure [kPa] |
|---|---|---|
| M100K104 | Warp | 20 |
| | | 40 |
| | Weft | 20 |
| | | 40 |
| YEM1801 | Warp | 10 |
| | | 15 |
| | Weft | 15 |
| | | 20 |

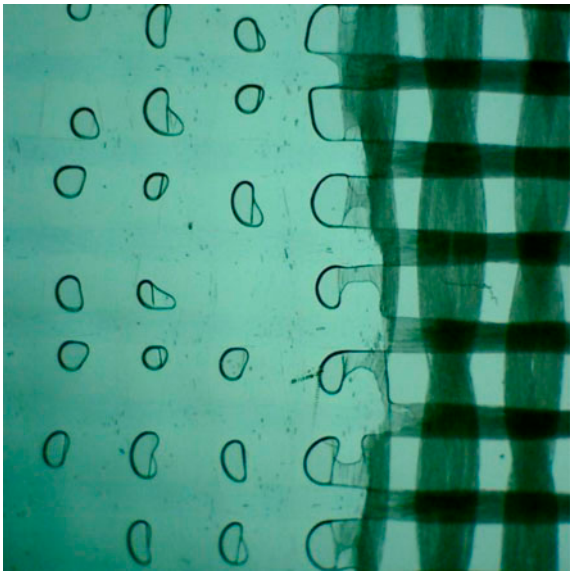

Figure 3. Microscopic image of voids observed with process visualization.

the experiments provided one layer, the thickness of which was comparatively smaller than the diameter of the generated voids. Thus, the content of voids by area was treated as their volume content.

### 3.2. *Results and discussion*

The relationship between the position from the resin inlet, $x$, and the arrival time $t$ of the flow front to position $x$ can be approximated with a quadratic function according to one-dimensional flow case of Darcy's law [21]:

$$t = \frac{\mu}{2kp}x^2 \tag{1}$$

where $k$ is the fabric permeability, $p$ is the injection pressure, and $\mu$ is the resin viscosity. The average permeabilities $k$ of the warp and weft directional impregnation of YEM1801 and M100K104 obtained by fitting the quadratic function to the relationship between position $x$ and arrival time $t$ are shown in Figure 4.

For both woven fabrics, the permeability of the warp direction was larger than that in the weft direction. This was attributed to the cross-sectional shape of the anisotropic plain-woven fabrics as shown in Figure 5. With the anisotropic plain-woven fabric consisting of narrow and thick fiber bundles in the warp direction, and wide and thin fiber bundles in the weft direction, the gap between the fiber bundles in the cross section was larger in the warp direction (Figure 5(b)). Therefore, because the drag resistance was smaller in the warp direction, flow through the woven networks was relatively easy. YEM1801 had larger permeability than M100K104 in both the warp direction and the weft direction. This was because the thickness of the fiber bundles and the distance between them were larger in YEM1801; thus, the gap between fiber bundles in the cross-section of YEM1801was larger than that of M100K104.

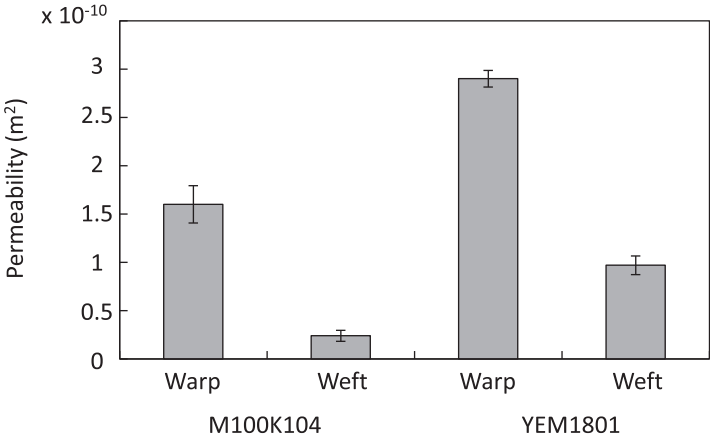


Figure 4. Measured permeabilities in warp and weft directions of fabrics M100K104 and YEM1801.

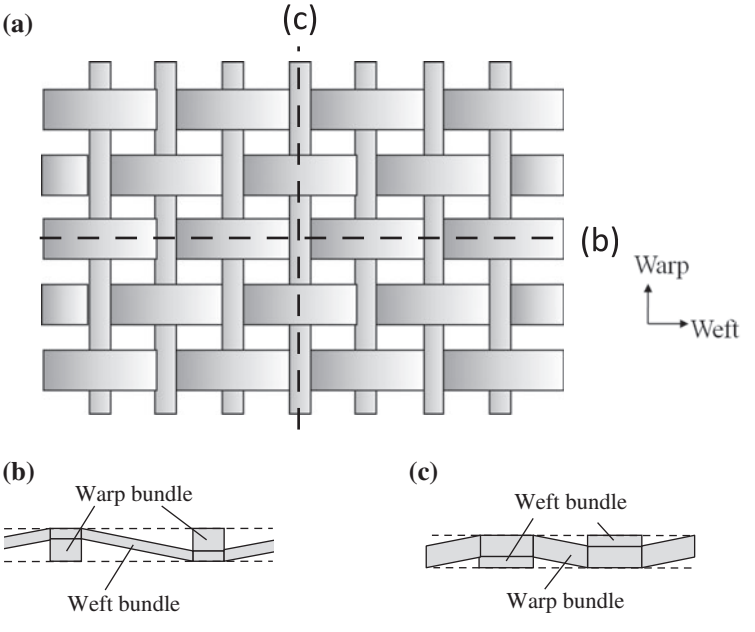


Figure 5. Configurations of geometry–anisotropic plain woven fabric. (a) Overall structure. (b) Cross-section in warp direction. (c) Cross-section in weft direction.

Figures 6 and 7 shows the relationship between the distance from the resin inlet and the void content at each measurement position of M100K1046 and YEM1801, respectively. It should be noted that the void content on the ordinate was measured *in situ* just after void entrapment; it does not include the effect of void transportation or volume change due to surrounding pressure change on the void content.[21] Regardless of the woven fabric type or the direction of impregnation, the void content increased as the distance from the resin inlet increased. Moreover, when comparing at the same

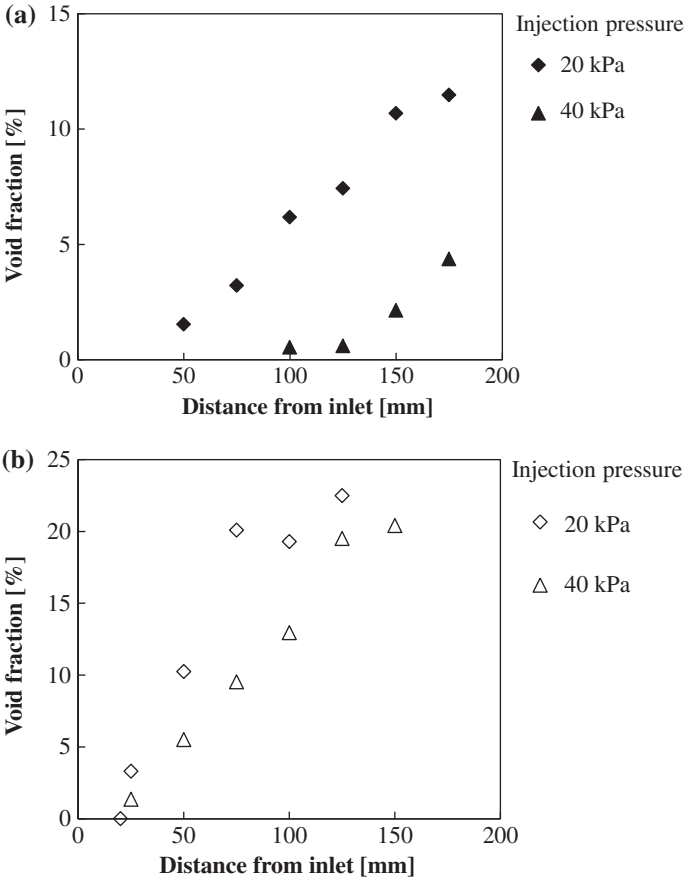


Figure 6. Void content measured at each position of M100K104. (a) Warp directional impregnation. (b) Weft directional impregnation.



measurement position, the void content was greater in the case of smaller injection pressure. This was because as the distance from the resin inlet became large or the injection pressure became small, the resin flow velocity decreased, which induced the dominance of the capillary pressure over hydrostatic pressure and precedence of resin impregnation inside the fiber bundles, thus possibly causing the larger inter-bundle void.

Figures 8 and 9 shows the relationship between the flow front velocity and the void content of the woven fabric M100K104 and YEM1801, respectively. Here, the flow velocity was computed by Darcy's law using the permeability obtained experimentally as shown in Figure 4. Qualitative coincidence was observed in the results shown in Figures 8 and 9. That is, in each woven fabric and each impregnation direction, the relationship between the flow front velocity and void content did not depend on the resin injection pressure, and could be expressed by one approximated line. From the vertex of the approximated line and the horizontal axis, the critical resin flow velocity $U_0$ at which the void content became zero could be obtained and is shown in Table 3. The critical flow velocity $U_0$ of the void formation in the warp directional impregnation was higher than that in the weft directional impregnation. Moreover, the void content at

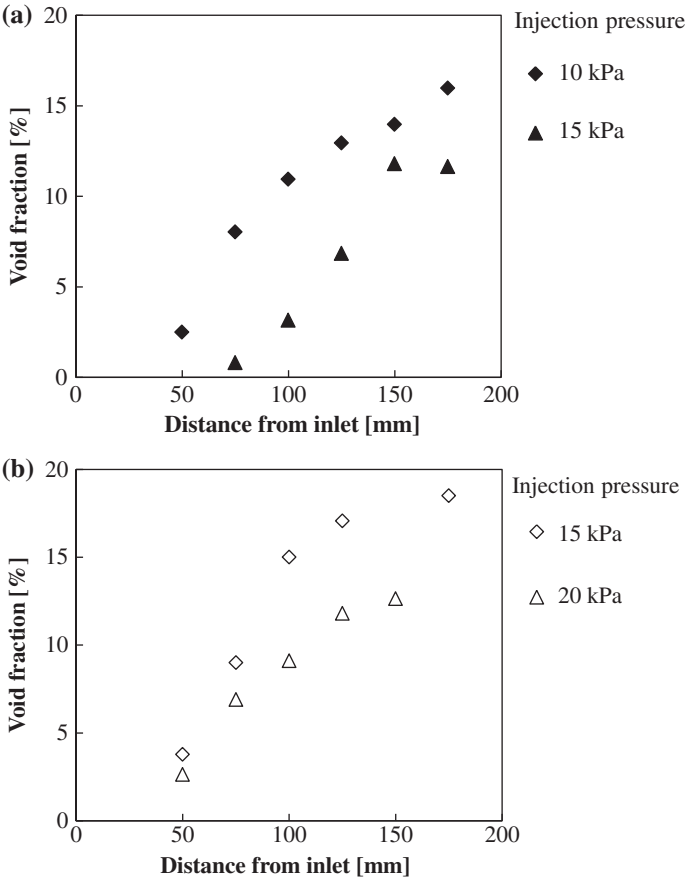


Figure 7. Void content measured at each position of YEM1801. (a) Warp directional impregnation. (b) Weft directional impregnation.

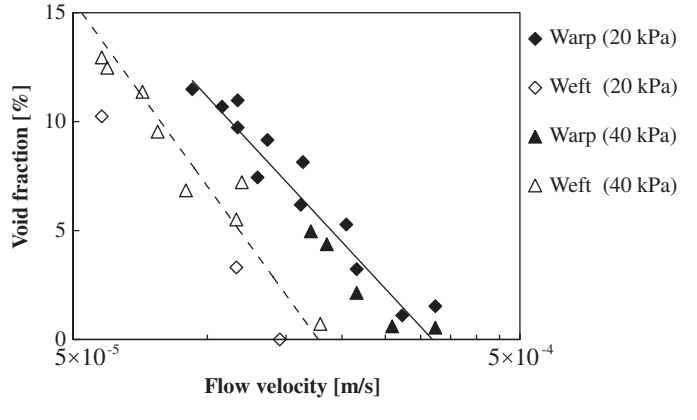


Figure 8. Void content vs. flow velocity in warp and weft impregnation directions of M100K104.

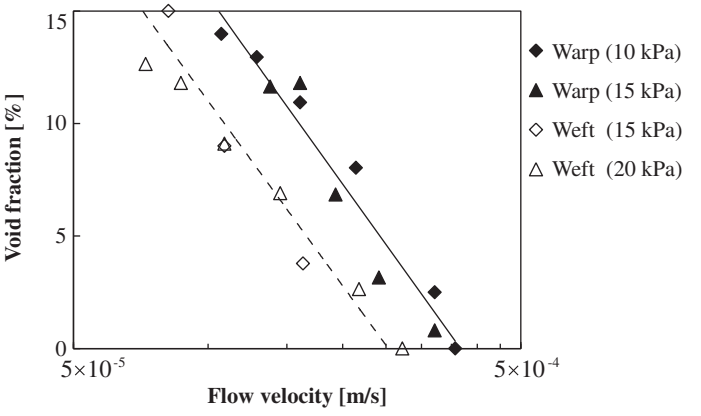


Figure 9. Void content vs. flow velocity in warp and weft impregnation directions of YEM1801.

Table 3. Critical flow velocity for void prevention obtained from experiments.

| Woven fabric | Flow direction | Critical flow velocity $U_0$ [m/s] |
|---|---|---|
| M100K104 | Warp | $3.2 \times 10^{-4}$ |
| | Weft | $1.8 \times 10^{-4}$ |
| YEM1801 | Warp | $3.7 \times 10^{-4}$ |
| | Weft | $2.5 \times 10^{-4}$ |

the same flow front velocity in the warp impregnation was greater than that in the weft impregnation. These results indicate that the void content depends on the direction of impregnation in addition to the flow front velocity in the geometry–anisotropic woven fabrics.

## 4. Mechanism of inter-bundle void formation

To clarify the mechanism of void formation, a picture of the microscopic resin progress and void formation at the flow front in woven fabrics (M100K104) was taken and is shown in Figure 10. The woven fabric was impregnated in the warp direction with the resin injection pressure of 40 kPa. In Figure 10(a) and (b), the observation position is $x = 75$ and 125 mm from the resin inlet, corresponding to the macroscopic flow front velocities $U = 1.2 \times 10^{-3}$ and $0.32 \times 10^{-3}$ m/s, respectively.

In the comparatively high-flow velocity zone (Figure 10(a)), a void did not occur, whereas in the low-flow velocity zone (Figure 10(b)), an inter-bundle void occurred. The microscope images indicate that the formation mechanism of the inter-bundle void consisted of the following two steps:

(1) Under the low-flow velocity, because of the dominance of the capillary force, the capillary fingering (lead-lag) phenomenon occurs, in which the intra-bundle flow precedes the inter-bundle flow.
(2) The preceded intra-bundle flow reaches the transverse fiber bundle, and resin flow occurs in the transverse direction; then, the two transverse flows encounter each other.

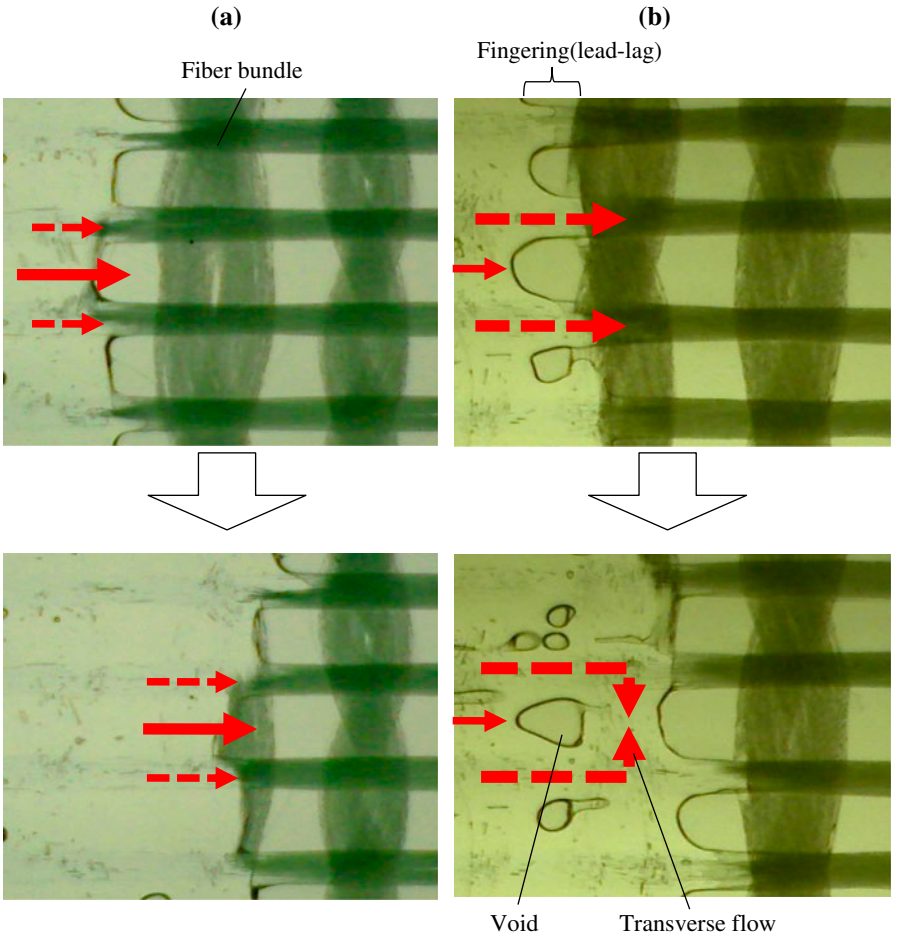


Figure 10. Microscopic observation of flow front of M100K104 under (a) high-flow velocity ($1.2 \times 10^{-3}$ m/s) and (b) low-flow velocity ($0.32 \times 10^{-3}$ m/s).

Because the transverse flow impregnated the transverse bundle before the inter-bundle flow filled the inter-bundle space, an air bubble was trapped in the inter-bundle space and remained as a void. Thus, inter-bundle void formation may have been affected by two phenomena: (1) fingering generation and (2) impregnation in the transverse fiber bundle.

As shown in Figures 8 and 9 and in the geometry–anisotropic woven fabrics, the void content under a certain resin flow velocity changed with the direction of resin impregnation. This implies that either or both of the above phenomena (1) and (2) was/were affected by the anisotropic geometry of the woven fabric.

Regarding phenomenon (2), as the distance between adjacent fiber bundles in the direction of macroscopic flow became small, the resin impregnation in the transverse direction completed in a shorter time. Because the distance between the fiber bundles in the weft direction, $L_{warp}$, was smaller than that in the warp direction, $L_{weft}$, resin impregnation in the transverse direction completed in a shorter time than weft impregnation. This may have caused a larger void in weft impregnation than in warp impregnation. However, this would contradict the experimental results as shown in Figures 8 and 9.

Therefore, fingering generation (1) may have had a larger influence on the void content and the critical flow velocity of the void formation than transverse impregnation (2). Thus, the effect of the direction of the resin impregnation on fingering generation was investigated in detail as described in the next section.

## 5. Measurements of flow velocity upon fingering occurrence

### *5.1. Experimental*

To evaluate the position and the flow velocity upon fingering occurrence, the distance was measured from the resin inlet when the intra-bundle flow preceded the inter-bundle flow and fingering occurred. The distance of fingering formation was measured by adjusting the direction of the resin impregnation of the woven fabrics to warp and weft. To observe the flow front microscopically, the microscope was moved along with the flow front, and the flow front was recorded as an animation. M100K104 was used for the woven fabric, and unsaturated polyester (Sundhoma PC184-C, DH Material Inc.) mixed with hardening agent (Epoch PN) at 1 PHR was used for the resin. The injection pressure was maintained at 20 or 40 kPa during impregnation.

### *5.2. Results and discussion*

Figure 11 shows the distance from the resin inlet when capillary fingering occurred at the flow front under each experimental condition. The error bar indicates the standard deviation of three measurements. Note that the leading flow front of the fingering consisted of two types of flow as judged from the image of the fingering: the intra-bundle flow, and the flow inside the gap between the fiber bundle and the mold surface. Because the air bubble was trapped by the fingering penetration including these two flows, fingering was identified by observing this fingering penetration. When compared with the same direction of resin impregnation, the distance from the resin inlet when fingering occurred became larger as the resin injection pressure increased. This was because, as the resin injection pressure increased, the flow front velocity at the certain

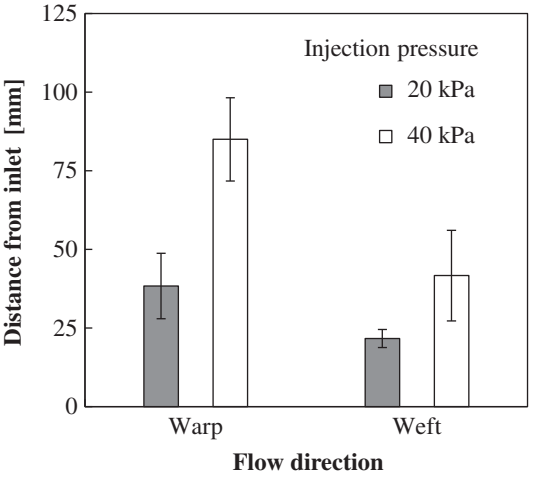


Figure 11. Distance from resin inlet to where capillary fingering is formed (M100K104).

distance from the resin inlet increased. This led to a decrease in the influence of the capillary force, and therefore fingering formation became more difficult.

Figure 12 shows the critical (i.e. maximum) flow velocity of fingering formation under each experimental condition. Resin flow velocity was calculated with Darcy's law and the permeability shown in Figure 4. It was found that the resin flow velocities when the fingering was formed were almost the same in each resin impregnation direction. This indicates that the formation of the fingering in each impregnation direction was dominated by the resin flow velocity regardless of the injection pressure. In addition, the critical flow velocity of the fingering formation was higher in the warp directional impregnation than that in the weft direction.

The velocity of the fingering formation was higher than the critical flow velocity of void formation ($3.2 \times 10^{-4}$ m/s) as shown in Table 3 in the warp directional impregnation. In the warp directional impregnation, the transverse distance between the adjacent warp fiber bundles was comparatively large, and the transverse flow required a longer time for impregnation than in the case of the weft directional impregnation. Therefore, a void may not form even though fingering occurs between the two critical velocities of fingering formation and void formation. On the other hand, in the case of the weft directional impregnation, because the distance between the adjacent weft fiber bundles was small, the two critical flow velocities of fingering and void formation were almost in agreement.

Figure 13 shows a comparison of the flow front configuration of each resin impregnated direction observed under the same resin flow velocity ($U = 2.3 \times 10^{-4}$ m/s) between the two critical flow velocities of fingering formation in the warp and weft impregnations. In the case of the warp directional impregnation, the intra-bundle flow preceded the inter-bundle flow greatly and fingering penetration occurred, whereas in the case of weft directional impregnation, precedence of the intra-bundle flow was scarcely observed, and the resin did not fully impregnate through the thickness, and complete fingering did not occur.

Because there was no difference in the properties inside the warp and weft fiber bundles, such as the fiber content in a single fiber bundle, the area of the fiber bundle,

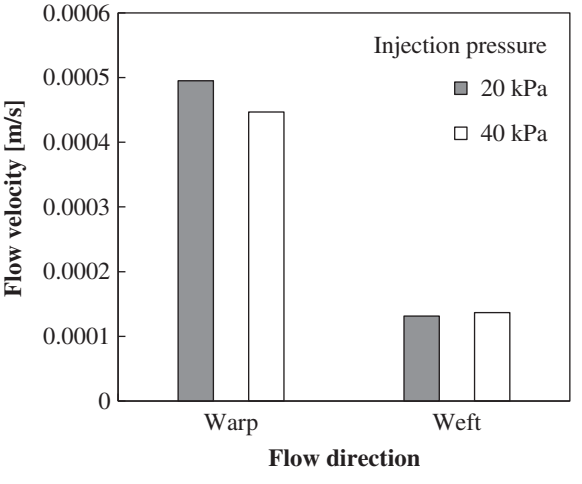


Figure 12. Critical flow velocities when capillary fingering is formed (M100K104).

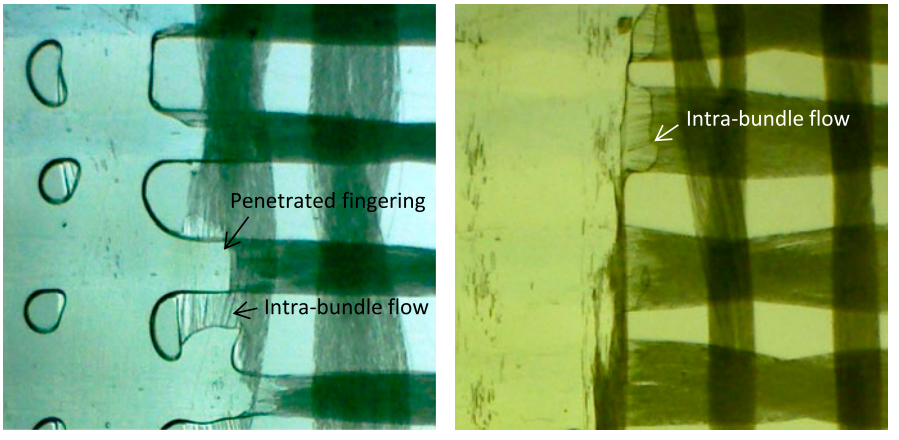


Figure 13. Flow front shape in geometry–anisotropic woven fabric (M100K104) under flow velocity $U = 2.3 \times 10^{-4}$ m/s. (a) Warp directional impregnation. (b) Weft directional impregnation.

and the diameter of a single filament, the porous structures of the warp and weft fiber bundles almost agreed with each other. This means that the capillary force and the permeability (i.e. the fingering characteristics) inside the fiber bundle were the same in the warp and weft fiber bundles. Therefore, the difference in the critical flow velocity of the fingering formation between the warp and weft directions may be attributed to the gap between the fiber bundle and the mold surface.

Figure 14 shows a schematic of the cross-section and resin advancement in warp and weft resin impregnation directions in the geometry–anisotropic woven fabrics. Compared with the weft fiber bundle, the warp fiber bundle was narrower and thicker. Therefore, as shown in Figure 14(a), the mean gap between the fiber bundle and the mold surface in the warp directional impregnation was smaller than that in the weft directional impregnation. This indicates that the capillary pressure between the fiber bundle and the mold surface became larger in the warp directional impregnation than that in the weft directional impregnation. Therefore, the flow velocity between the fiber bundle and mold surface may approach the intra-flow velocity, and fingering penetration was more easily formed in the warp directional impregnation. On the other hand, the mean gap between the fiber bundle and the mold surface was comparatively large in the weft directional impregnation; thus, the resin flow between the fiber bundle and the mold surface may delay from the intra-bundle flow, and fingering penetration was not

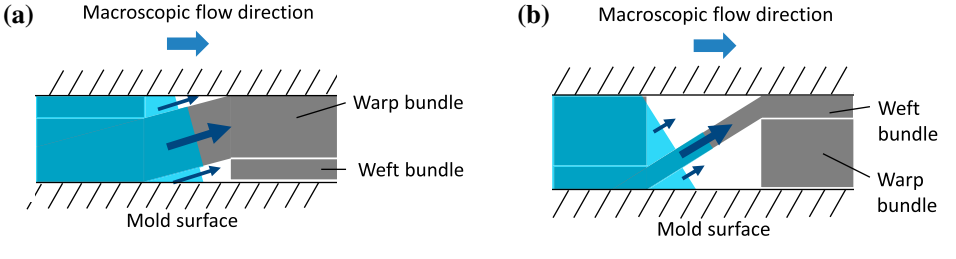


Figure 14. Influence of gap between fiber bundle and mold surface on flow advancement. (a) Warp directional impregnation. (b) Weft directional impregnation.

observed (Figure 14(b)). Therefore, the higher critical flow velocity of fingering formation in the warp directional impregnation than that in the weft directional impregnation is attributed to the difference of the capillary pressure inside the gap between the fiber bundles and the mold surface. In addition, this may lead to a higher critical velocity of void formation and a higher void content at a given flow velocity in the case of warp directional impregnation. To verify this quantitatively, future work will conduct mathematical modeling to predict void and fingering formation including the effects of the gap between the fiber bundles and mold surface.

## 6. Conclusions

This study investigated the influence of geometric anisotropy of woven fabrics on the relationship between void generation and resin flow velocity during RTM. The relationship between void content and resin flow velocity was measured in warp (narrow and thick bundle) and weft (wide and thin bundle) directional impregnation. The warp directional impregnation indicated a higher critical resin flow velocity of void formation and a higher void content under a given resin flow velocity than those in the weft directional impregnation.

When observed with a microscope, it was found that the void was formed by capillary fingering and transverse resin flow in the flow front. Of these two factors, fingering generation had a greater influence on void generation. Comparing the warp and weft directional impregnations, the warp directional impregnation indicated a higher critical flow velocity of fingering formation. This can be explained by the fact that the gap between a fiber bundle and the mold surface is smaller in the warp direction; thus, the capillary force is higher, and the critical flow velocity of fingering formation increases. This may also lead to a higher critical velocity of void formation and a higher void content at a given flow velocity in warp directional impregnation.



## References

[1] Kruckenberg TM, Paton R. Resin transfer moulding for aerospace structures. Dordrecht: Springer; 1998.
[2] Matsuzaki R, Kobayashi S, Todoroki A, Mizutani Y. Control of resin flow/temperature using multifunctional interdigital electrode array film during a VaRTM process. Compos. A. 2011;42:782–793.
[3] Matsuzaki R, Kobayashi S, Todoroki A, Mizutani Y. Flow control by progressive forecasting using numerical simulation during vacuum-assisted resin transfer molding. Compos. A. 2013;45:79–87.
[4] Huang H, Talreja R. Effects of void geometry on elastic properties of unidirectional fiber reinforced composites. Compos. Sci. Technol. 2005;65:1964–1981.
[5] Varna J, Joffe R, Berglund LA. Effect of voids on failure mechanisms in RTM laminates. Compos. Sci. Technol. 1995;53:241–249.
[6] Ghiorse SR. Effect of void content on the mechanical properties of carbon/epoxy laminates. SAMPE Q. 1993;24:54–59.
[7] Matsuzaki R, Kobayashi S, Todoroki A, Mizutani Y. Full-field monitoring of resin flow using an area-sensor array in a VaRTM process. Compos. A. 2011;42:550–559.
[8] Park CH, Lee WI. Modeling void formation and unsaturated flow in liquid composite molding processes: a survey and review. J. Reinf. Plast. Compos. 2011;30:957–977.
[9] Patel N, Lee LJ. Effects of fiber mat architecture on void formation and removal in liquid composite molding. Polym. Compos. 1995;16:386–399.
[10] Rohatgi V, Patel N, Lee LJ. Experimental investigation of flow-induced microvoids during impregnation of unidirectional stitched fiberglass mat. Polym. Compos. 1996;17:161–170.

[11] Kang MK, Lee WI, Hahn HT. Formation of microvoids during resin-transfer molding process. Compos. Sci. Technol. 2000;60:2427–2434.
[12] Lundstrom TS, Gebart BR. Influence from process parameters on void formation in resin transfer molding. Polym. Compos. 1994;15:25–33.
[13] Patel N, Lee LJ. Modeling of void formation and removal in liquid composite molding. 2. Model development and implementation. Polym. Compos. 1996;17:104–114.
[14] Patel N, Lee LJ. Modeling of void formation and removal in liquid composite molding. 1. Wettability analysis. Polym. Compos. 1996;17:96–103.
[15] Patel N, Rohatgi V, Lee LJ. Micro scale flow behavior and void formation mechanism during impregnation through a unidirectional stitched fiberglass mat. Polym. Eng. Sci. 1995;35:837–851.
[16] Leclerc JS, Ruiz E. Porosity reduction using optimized flow velocity in Resin Transfer Molding. Compos. A. 2008;39:1859–1868.
[17] Schell JSU, Deleglise M, Binetruy C, Krawczak P, Ermanni P. Numerical prediction and experimental characterisation of meso-scale-voids in liquid composite moulding. Compos. A. 2007;38:2460–2470.
[18] Frishfelds V, Lundström TS, Jakovics A. Bubble motion through non-crimp fabrics during composites manufacturing. Compos. A. 2008;39:243–251.
[19] Lundstrom TS. Bubble transport through constricted capillary tubes with application to resin transfer molding. Polym. Compos. 1996;17:770–779.
[20] Lundstorm TS. Measurement of void collapse during resin transfer moulding. Compos. A. 1996;28:201–214.
[21] Matsuzaki R, Seto D, Todoroki A, Mizutani Y. In-situ void content measurements during resin transfer molding. Adv. Compos. Mater. 2013;22:239–254.